Available online at www.sciencedirect.com
ScienceDirect
Applied Catalysis B: Environmental 83 (2008) 1–7
APPLIED CATALYSIS B: ENVIRONMENTAL
www.elsevier.com/locate/apcatb

Photocatalytic TiO_2 thin films by aerosol-deposition: From micron-sized particles to nano-grained thin film at room temperature

Jungho Ryu, Dong-Soo Park *, Byung-Dong Hahn, Jong-Jin Choi, Woon-Ha Yoon, Kun-Young Kim, Hui-Suk Yun

Center for Future Technology, Korea Institute of Materials Science (KIMS), 66 Sangnam-Dong, Changwon, Kyungnam 641-831, Republic of Korea

Received 25 August 2007; received in revised form 18 January 2008; accepted 26 January 2008
Available online 5 February 2008

Abstract

A nano-sized, TiO_2 photocatalytic thin film with a dispersion of anatase crystallites was successfully fabricated from a micron-sized powder by aerosol deposition (AD) at room temperature (RT). Extremely rough, network-structured, photocatalytic thin films were obtained without any binder or heat treatment. The films were photocatalytically active under both ultraviolet (UV) and solar light as a result of their nano-sized, anatase grains and amorphous phase. Various photocatalytic evaluations confirmed the excellent photocatalytic performance of the AD TiO_2 film in terms of organic degradation, pathogen disinfection, and hydrophilicity. This enhanced photocatalytic performance was attributed not only to the nano-crystalline anatase grains, but also to the exceptionally rough, network microstructure and nano-projections capable of supporting the enhanced loading of organic contaminants onto the film surface. Furthermore, because the nano-grained, AD TiO_2 photocatalytic thin films were fabricated from low-cost, micron-sized powder with a deposition rate as high as 3 μm/min at RT, this process promises to be one of the most cost-effective methods for many practical photocatalyst applications.

Keywords: Anatase; TiO_2; Thin film; Aerosol deposition; Photocatalyst

1. Introduction

Serious attention has been focused on the photocatalytic performance of TiO_2, due to its good environmental stability, for the purification of contaminated air or water [1–5], deodorization and bactericidal treatment [6–11], and use in self-cleaning coatings [12]. In the early research on the TiO_2 photocatalyst, most investigations focused on the powder-form photocatalyst. However, drawbacks are encountered with powder suspensions, which render the powder-form photocatalyst unsuitable for use under flowing fluid systems and difficult to reuse because of difficult separation of TiO_2 particles from the suspension and easy aggregation of suspended TiO_2 particles [1,13], To overcome these drawbacks of the powder-form photocatalyst, many investigations have therefore focused on thin/thick film forms of photocatalytic TiO_2 [9–18]. The several methods available for the fabrication of TiO_2 photocatalytic films include sol–gel [14–16], sputtering [11,17,18], e-beam evaporation [19], and metal organic chemical vapor deposition (MOCVD) [20]. It is well known that to improve the photocatalytic effect of TiO_2, the grain/particle size must be reduced to nanometer scale with an anatase phase crystalline structure and high specific surface area [1,21].

Aerosol deposition (AD) is a kind of gas deposition method using fine particles mixed with a carrier gas to form a colloid aerosol flow [22–26]. The aerosol flow is accelerated by the high-pressure difference between two chambers and ejected through a nozzle. The particles accelerated in the aerosol flow collide at subsonic speed onto the substrate and form a dense and nano-crystalline ceramic film at room temperature (RT). One of the important advantage of the AD is there are no compositional changes or phase transition during process. Therefore to form the nano-crystalline anatase film by AD, the initial powder should be crystalline anatase phase. The other attractive advantage of AD is the deposition of dense ceramic

* Corresponding author. Tel.: +82 55 280 3345; fax: +82 55 280 3389.
E-mail address: pds1590@kims.re.kr (D.-S. Park).

0926-3373/$ – see front matter
doi:10.1016/j.apcatb.2008.01.020

films at RT with high deposition rate. In our previous reports, we prepared several ceramic films such as piezoelectric/ferroelectric materials [24,25] and electrically conductive materials for fuel cell application [26] by AD. Most of the as-deposited films were very dense (over 95% relative density) with a complex composite microstructure of nano-crystallite with amorphous phase [24–26]. Therefore, we can expect the use of AD for anatase TiO_2 thin film to be very effective for the preparation of nano-grained anatase TiO_2 thin films at RT. As AD's deposition rate is exceptionally higher (several microns to hundreds of microns/min) than that of any other thin film process, and as it uses inexpensive, (sub-)micron-sized, raw powders rather than expensive, nano-sized powders, this method is cost-effective for the production of TiO_2 photocatalytic film for practical applications. In this study, we propose a cost-effective technique for the fabrication of high quality, anatase TiO_2 photocatalytic thin films at RT. The TiO_2 thin films with nano-grained anatase mixed in an amorphous phase with an exceptionally rough network microstructure were successfully fabricated from micron-sized powder at RT by AD. To clarify the film performance, the photocatalytic performance of the fabricated films was evaluated by measuring the photo-degradation of methylene blue (MB) aqueous solution, bactericidal test with *Escherichia coli* (*E. coli*), and water contact angle changes.

2. Experimental

2.1. TiO_2 film fabrication

The raw powder used in the study was capacitor grade TiO_2 powder of anatase rich phase (TA-540, Shanghai SMEC Corp., Shanghai, China. d_{50} ~2.41 μm, and purity 98.6%). The average particle sizes of the powders were measured by laser diffraction particle size analyzer (HELOS & RODOS, Windox 5, Sympatec GmbH, Clausthal-Zellerfeld, Germany). The raw powders were mixed with the carrier gas in the aerosol chamber to form an aerosol flow which was transported through a tube to a nozzle, accelerated and ejected from a nozzle with rectangular shaped orifices of 25 mm × 1.0 mm into a deposition chamber, which was evacuated by a rotary pump with a mechanical buster. Oxygen gas with purity of 99% was used as the carrier gas at a flow rate of 30 l/min. During deposition the pressure of the aerosol chamber was ~600 Torr, while that of the deposition chamber was ~4 Torr. The accelerated TiO_2 particles collided with the glass (Corning 1737) substrate, which was located 5 mm from the nozzle, and formed a dense TiO_2 film at RT. The area of the deposited film was ~50 mm × 50 mm, and the maximum deposition rate was ~3 μm/min. The film thickness was controlled in the range of 3–5 μm by the number of repetitions of the nozzle scan. The color of the AD film was yellowish dark gray. To investigate the feasibility for practical applications, TiO_2 films were deposited on various substrates such as sand blasted stainless steel plates, Ni and Cu sponges, ceramics balls, ceramics tiles, and polycarbonates plates (photos of the samples are illustrated in supplementary data). Since the AD mechanism is related with kinetic and fracture energy of the particle [22], the optimized deposition behavior was obtained from the powders have average particle size (d_{50}) of 2–3 μm. Other commercial photocatalytic TiO_2 powders such as nano-crystalline Degussa's P-25 and Nano Co. Ltd.'s NT-22 were not deposited on the substrates but formed powder compacts by AD due to the lower kinetic energy which is related with particle size.

2.2. TiO_2 film characterization

The phases of the starting powders and deposited films were identified by X-ray diffractometry (XRD: D-MAX 2200, Rigaku Co., Tokyo, Japan) with Cu Kα radiation with an angular domain between 20° and 60° (2θ). The microstructures of the raw powder and films were observed using scanning electron microscopy (SEM: JSM-5800, JEOL Co., Tokyo, Japan) operating at 15 kV and transmission electron microscopy (TEM: JEM-2100F, JEOL Co., Tokyo, Japan) operating at 200 kV. For the raw powder observation by TEM, small powder clusters were selected for the diffraction patterns and bright field image due to the limited penetration depth of the electron beam. The surface roughness and adhesive strength of the film were measured using a surface roughness profiler (MarSurf XR 20, Mahr GmbH, Goettingen, Germany) and universal testing machine (Instron series IX automated materials testing system, Instron Corp. MA, USA), respectively. The surface roughness (R_a, R_z, and R_{max}) was measured 5 times for each sample with a scanning distance of 4 mm at different positions. To measure the adhesive strength between the film and substrate, the films were coated on a stainless steel substrate (Ø 18 mm and t 0.5 mm) and fixtures were bonded on the film's top side and substrate's bottom side with thermal cure, high strength epoxy (3 M Scotch-Weld Epoxy Adhesive 2214, 3 M Corp., MN, USA) and cured at 150 °C for 24 h. The adhesive strength test was conducted according to ASTM C633, with bonding area and crosshead speed of Ø 18 mm and 1 mm/min, respectively. The optical absorption spectra were taken from the film, raw powder and two commercially available TiO_2 photocatalytic powders, NT-22 (Nano Co. Ltd., Jinju, Korea) and P-25 (Degussa GmbH, Germany), by using diffuse reflectance mode of ultraviolet (UV)–vis spectrophotometer (Cary 500, Varian Inc., Palo Alto, CA, USA). The reflectance data was converted to the absorbance according to the Kubelka-Munk function [21].

2.3. Photocatalytic characterization

The degradation of MB aqueous solution (0.0005 wt% in water) by TiO_2 AD film was measured to determine the film's photocatalytic capabilities. MB solution (#319112, 0.05 wt% solution in water, Aldrich Chemical Co., MO, USA) was diluted with de-ionized water at a volume ratio of 1:100. The TiO_2 films and 300 ml of MB solution were put into a Pyrex vessel, covered by a Pyrex Petri dish and illuminated at a distance of 20 cm with a 1 kW, high-pressure UV metal (Fe) lamp working in the main wavelength of 365 nm. The UV intensity at the film surface was ~10 mW/cm^2. To determine the photocatalytic capability of the film under solar illumina-

tion, the Pyrex vessel with MB solution and film was left on the terrace of the building under fine weather condition with a temperature variation of 18–23 °C during illumination. A small amount of MB solution (~5 ml) was taken from the vessel after 0.5, 1, and 2 h of UV illumination and after 2, 4, and 6 h solar illumination time. The UV–vis spectra of the MB solutions were measured to check for MB degradation by using a UV–vis spectrophotometer. The bactericidal activity of the TiO_2 film was evaluated using the antibacterial drop-test. TiO_2 films were exposed under UV illumination (1.0 mW/cm^2, 310–400 nm) for 30 min and the bacterial solutions (*E. coli* ATCC 25922) were then dropped and covered by transparent film. The inoculated film was illuminated by the same UV light source for another 1 h. For a negative control, another inoculated film was also tested without UV illumination. The inoculated films were washed by buffer solution and the remaining *E. coli* clusters were counted. Wetting angle measurements were performed to characterize the film's hydrophilicity. After being stored in the dark for at least 2 days, the films were exposed to UV for 5, 10, and 30 min. The UV light source condition was the same as that for the MB degradation measurement. After each illumination, each sample was mounted on the table of the contact angle measurement system (Phoenix 300 and Image XP ver. 5.0, Surface Electro Optics Co., Suwon, Korea). A 30-μl droplet of DI water was placed on its surface and the first contact angle was measured immediately.

3. Results and discussion

Fig. 1 shows the surface SEM micrographs of the AD TiO_2 films. A well developed network microstructure was observed in the film, along with the absence of any micro-cracks or pores. The film thickness was 3–5 μm. The deposited films maintained good adhesion with the glass or stainless steel substrate and the film's adhesive strength for the latter was over 30 MPa. The maximum strength of the bonding epoxy that was used for the testing was 30 MPa and delamination occurred between the substrate and fixture, but not between the film and fixture. Nano-scale projections on the wall of the network were observed, as shown in Fig. 1(b). The average surface roughness (R_a) of the film was 0.581 μm (cf. $R_z = 4.384$ and $R_{max} = 5.035$ μm), which was almost 1–2 orders of magnitude higher than that of typical sputtered ($R_a \sim$ several tens nm)[18] or sol–gel derived ($R_a \sim$ several nm)[16] TiO_2 films and even higher than that of the film with a spinodal phase separation structure ($R_{max} \sim 2$ μm) [14,15]. This film was expected to have a very high surface area due to aforementioned extreme roughness and numerous nano-projections on the network walls. In general, an increased available surface area enhances the loading of organic contaminants onto the surface of the TiO_2 photocatalyst. Therefore, nano-sized, porous TiO_2 particles or films that have a rough surface, which gives a high surface area, have better photocatalytic performance [1,27–29]. To the best of our knowledge, no studies have yet reported on this kind of network comprising microstructured TiO_2 films with high mechanical adhesion strength.

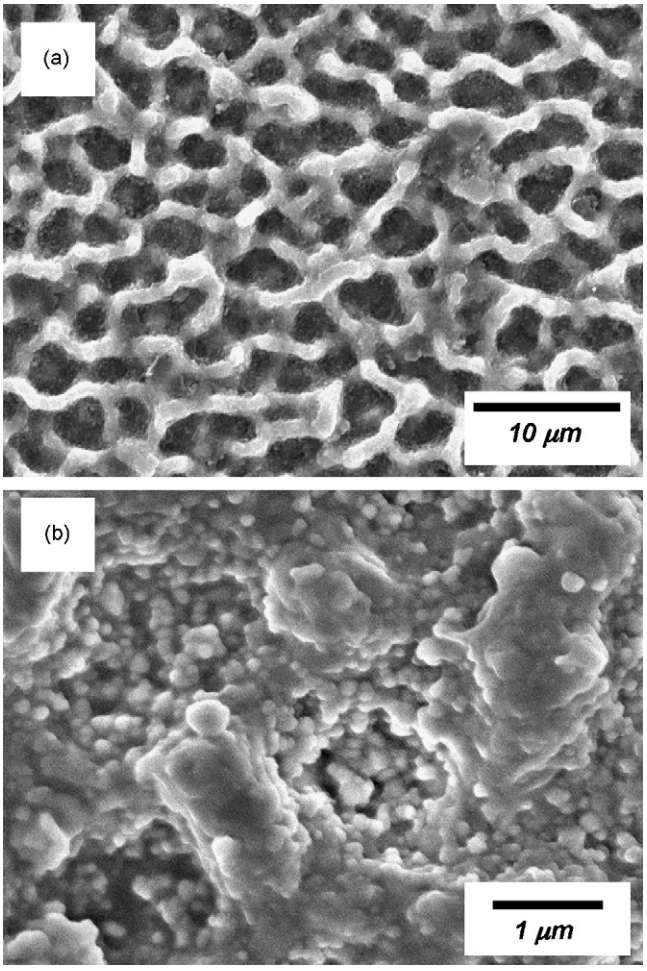

Fig. 1. SEM micrographs of TiO_2 film with network structure: (a) low and (b) high magnification images. Nano-projections are evident on the surface of the micro-network skeleton.

Bright field images and diffraction patterns of the raw powder and deposited TiO_2 film showed a clear difference in terms of crystallite sizes, as shown in Fig. 2. For the raw powder observation, small particle clusters were selected due to the limitation of the electron beam penetration depth. The raw powder consisted of a single crystalline. The average particle size of 2.41 μm was measured with a laser diffraction particle size analyzer. According to the manufacturer's specification sheet of TiO_2 raw powder, this powder is unsuitable for photocatalyst applications but can be applied to electric capacitors. Therefore, the primary particles are bigger than those of typical photocatalytic TiO_2 powder (typically d_{50} is 10–30 nm) and single crystalline. Moreover, the powder cost is only approximately 20% of that of typical, nano-sized, photocatalytic TiO_2 powder. The microstructure of the as-deposited film consisted of small, 5–30 nm sized crystallites with an amorphous phase (highly disordered phase) formed by collision of the accelerated particles with high kinetic energy during deposition.

The diffraction patterns from the TEM images of the film (Fig. 2(b) inset) showed clear evidence of the coexistence of nano-crystallites and amorphous phase. From the XRD

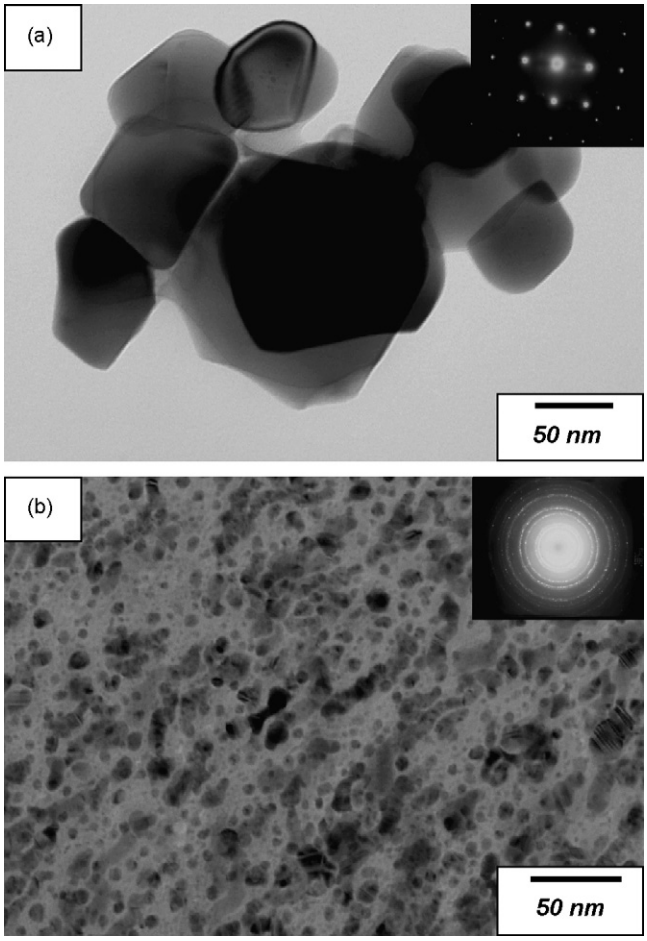

Fig. 2. TEM bright field images and electron beam diffraction patterns: (a) raw powder and (b) deposited film.

diffraction patterns (Fig. 3), crystallites were confirmed as mainly comprising anatase phase. The nano-projections seen in the SEM micrographs (Fig. 1(b)) were presumed to be small crystallites of anatase TiO_2.

The crystal phases of the powder and film prepared on the stainless steel substrate were characterized by XRD and are

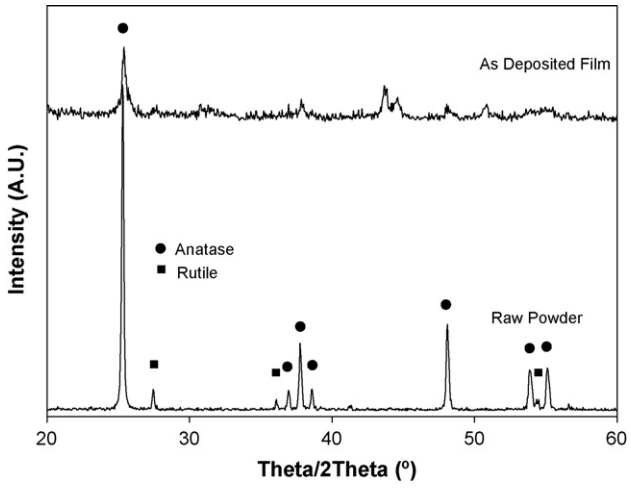

Fig. 3. XRD patterns of TiO_2 raw powder and deposited film.

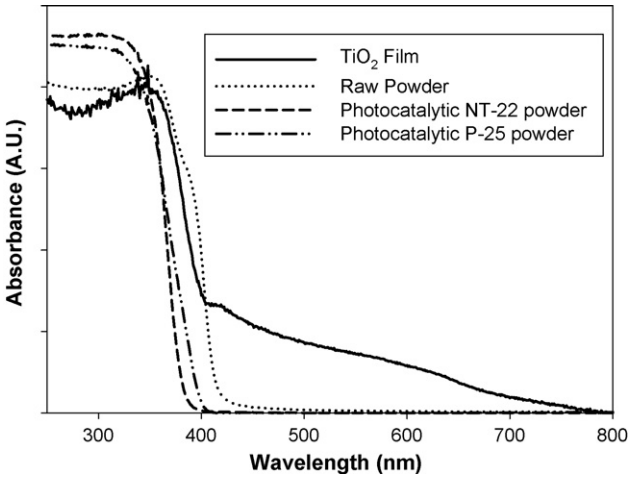

Fig. 4. Optical absorption spectra of TiO_2 raw powder and deposited film. For comparison with commercially available photocatalytic powder, NT-22 (Nano Co. Ltd., Korea) and P-25 (Deggusa GmbH, Germany) were measured.

depicted in Fig. 3. The initial starting TiO_2 powder was an anatase rich phase mixed with a small amount of rutile phase. The raw powder peaks were sharp and narrow, indicating a well crystallized phase with big grains. No other impurity phases except TiO_2 isomorphs phase were detected from the XRD patterns. The as-deposited film, however, showed small and broad peaks in comparison with the raw powder, despite being deposited at RT. According to the Scherrer relation, these broad XRD peaks imply that the film consisted of very small sized grains [24]. It is known that the high impact energy of the particle collisions occurring during deposition result in the small grain size of the films. This result was in good agreement with the TEM results (Fig. 2). It is worthy of notice that thermal treatment is essential for the fabrication of anatase phase TiO_2 thin films by other processes, whereas we achieved this by using AD at RT.

Fig. 4 shows the optical absorption spectra of the raw powder and AD film. To compare with commercially available photocatalyst powders, NT-22 (particle size 20–30 nm) from Nano Co. Ltd. and P-25 from Degussa were measured under the same condition. The crystal phases of NT-22 and P-25 were determined to be anatase phase from the XRD patterns. The raw TiO_2 powder used in this study showed strong absorption behavior at a wavelength of up to around 420 nm, while commercial photocatalytic powders and the film showed an absorption peak at less than 400 nm. All powders did not show absorption spectra in the vis range, however a shift of the absorbance thread to the vis region was observed for the AD TiO_2 film. Even though the absorbance of the film at vis region was lower than that under UV region, the AD TiO_2 film clearly demonstrated vis activity. As we aforementioned the sample displayed yellowish dark gray color and it might be due to this absorption of visible light, i.e. ~400 to ~700 nm wavelength. It is well known that yellowish color was observed from the vis active TiO_2 thin films or powders [17,18]. Bickley et al. have reported that the presence of the amorphous phase in a complex microstructure (mixed with anatase or rutile phase) contributes to moving the optical absorption tail toward high photocatalytic

activity due to the presence of localized Anderson states [30]. They suggested that the localized Anderson states of amorphous TiO_2 may increase the lifetime of photo-excited electron-hole pairs and thereby enhance the photocatalytic activity. Furthermore, the mixing of amorphous TiO_2 with anatase crystallite in the complex microstructure is expected to increase the vis activity, since the energy bandgap of amorphous TiO_2 (3.0 eV) is lower than that of the anatase phase (3.2 eV) [31]. In this regard, it is believed that the vis activity of the film may have been caused by the smaller energy bandgap of the amorphous phase which is mixed with anatase crystallite. In addition, AD is known to generate defects due to the high collision energy of the particles [22–26]. The oxygen or titanium defects which arise during the deposition process can also reduce the bandgap energy. From the above results, including microstructural evolution, crystal phase, and optical properties, the AD TiO_2 film is therefore expected to show superior photocatalytic properties to the films manufactured by other methods.

The optical absorption spectra of MB aqueous solutions photocatalytically degraded by AD TiO_2 films were measured using a UV–vis spectrophotometer. The photocatalytic degradations of MB under UV and solar illuminations are plotted in Fig. 5(a) and (b), respectively. Absorbance at all wavelengths from 800 to 250 nm decreased over time due to the MB degradation. Under UV light illumination, MB was rapidly degraded and the curve was completely flattened after irradiation for 2 h, as shown in Fig. 5(a). For the comparison, MB degradation by commercially available sol–gel derived photocatalytic thin film from Nano Co. Ltd. was measured under the same condition. The AD TiO_2 film has superior photocatalytic activity to that of the sol–gel derived TiO_2 film as shown in Fig. 5(a). Even 1 h irradiation condition, AD film showed superior MB degradation behavior to that of sol–gel film under 2 h irradiation condition. The photocatalytic degradation of MB was slower for solar illumination than for UV illumination. Even though the photocatalytic degradation rate under solar illumination was slower than that under UV illumination, the AD TiO_2 film clearly demonstrated photocatalytic capability under solar illumination.

Another useful and interesting photocatalytic ability of TiO_2 is the bactericidal effect, because they do not form dangerous

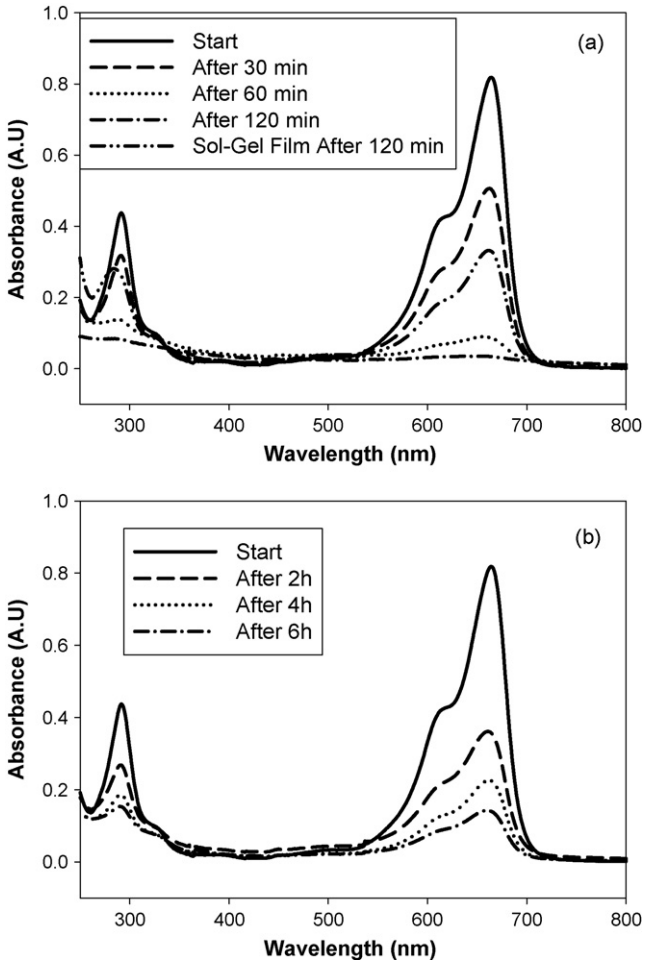

Fig. 5. UV–vis spectra of MB (0.0005 wt%)-DI water solution with TiO_2 film (50 mm × 50 mm) as a function of illumination time: (a) UV (main wavelength 365 nm) and (b) solar illumination.

compounds and present high efficiency disinfection [6–8,11]. We evaluated the photocatalytic bactericidal effect of AD TiO_2 film with *E. coli*. The inhibition rate of the tested *E. coli* was as high as 99.8% after 60 min of illumination. The concentration of *E. coli* strain was reduced from an initial 421 CFU/40 μl to 1 CFU/40 μl after 60 min of UV (wavelength 310–400 nm) irradiation. The differences between before and after bacter-

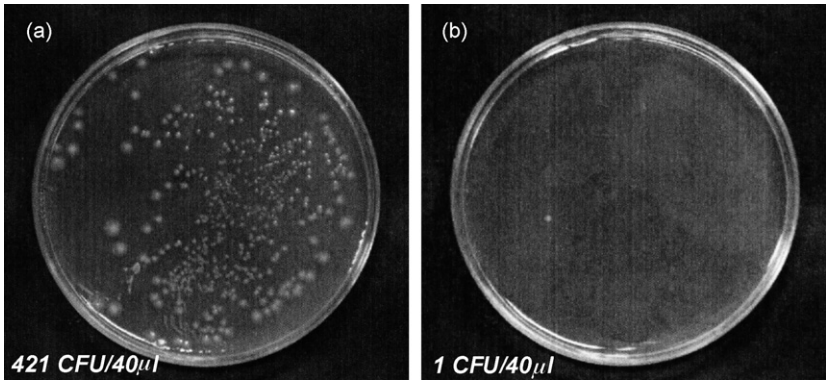

Fig. 6. Photographs of bactericidal test Petri dish with *E. coli* ATCC 25922 colonies: (a) before and (b) after UV (wavelength 310–400 nm) illumination for 60 min.

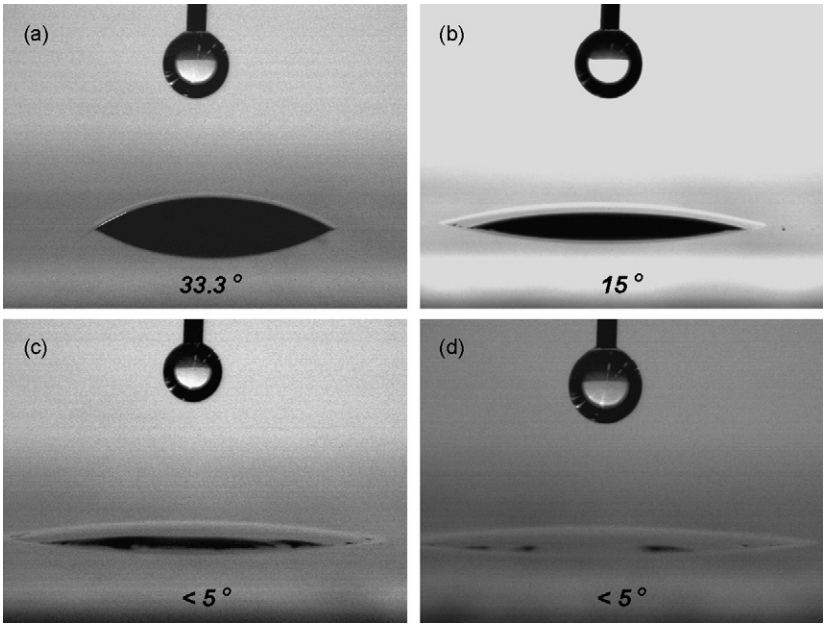

Fig. 7. Photographs of water wetting test after UV light (365 nm) exposure for (a) 0, (b) 5, (c) 10, and (d) 30 min. The wetting angles indicated noted at the bottom of each photo.

icidal testing were seen in the photos of the testing Petri dish, as illustrated in Fig. 6. The white spots in the Petri dish corresponded to the *E. coli* colonies used in the testing. The negative control sample did not show any changes in terms of the number or shape of *E. coli* colonies. This result confirmed that nearly complete disinfection occurred in the presence of AD TiO_2 thin film exposed to UV illumination after 60 min.

Recently, TiO_2 has been reported to exhibit hydrophilic and amphiphilic behaviors [12,32]. The hydrophilic property of the film surface allows water to spread completely across the surface rather than remaining as droplets. The results of this hydrophilic property are antifogging and the so-called self-cleaning effect of TiO_2 film. One of the most interesting aspects of TiO_2 is that the photocatalysis and hydrophilicity can take place simultaneously on the same surface even though the mechanisms are completely different [12,32]. This photo-induced hydrophilic behavior is known as an important self-cleaning application of TiO_2. In the last evaluation of the photocatalytic activity, we measured the contact angle of water on the AD films after a certain time of UV illumination. Fig. 7 shows the appearance of the samples with a surface wetted by water droplets (results of wettability testing). The result demonstrated the very quick response of the photo-induced hydrophilic behavior of the AD TiO_2 films. The contact angle of the TiO_2 film was initially around 33°, then decreased to 15° after 5 min UV irradiation, and further decreased to less than 5°, which was the lower limit of our measurement system, after 10 min UV irradiation.

4. Conclusion

In summary, nano-sized, TiO_2 photocatalytic thin film with a dispersion of anatase crystallites was successfully fabricated from micron-sized raw powder by AD at RT. Extremely rough, network structured, photocatalytic thin films were obtained without any heat treatment. AD TiO_2 films were photocatalytically active under both UV and in the solar region as a result of their nano-sized, anatase grains and amorphous phase. Exceptionally rough network microstructure and nano-projections able to support enhanced loading of organic contaminants onto the surface of the TiO_2 photocatalytic film were observed. Various photocatalytic evaluations of the AD TiO_2 film showed excellent photocatalytic performance in terms of organic degradation, pathogen disinfection, and hydrophilicity. Furthermore, as the nano-grained AD TiO_2 photocatalytic thin films were fabricated from low-cost, micron-sized powder with a deposition rate as high as 3 μm/min at RT, this process promises to be one of the most cost-effective for many practical photocatalyst applications, such as purification of contaminated air/water, pathogen inactivation, and self-cleaning ceramic tiles.

Appendix A. Supplementary data

Supplementary data associated with this article can be found, in the online version, at doi:10.1016/j.apcatb.2008.01.020.

References

[1] F. Kskandar, A.B.D. Nandiyanto, K.M. Yun, C.J. Hogan Jr., K. Okuyama, P. Biswas, Adv. Mater. 19 (2007) 1408–1412.
[2] M. Stylidi, D.I. Kondarides, X.E. Verykios, Appl. Catal. B 40 (2003) 271–286.
[3] D. Beydoun, R. Amal, G.K.C. Low, S. McEvoy, J. Phys. Chem. B 104 (2000) 4387–4396.
[4] J. Chen, M. Liu, L. Zhang, J. Zhang, L. Jin, Water Res. 37 (2003) 3815–3820.

[5] T.A. Egerton, P.A. Christensen, S.A.M. Kosa, B. Onoka, J.C. Harper, J.R. Tinlin, Int. J. Environ. Pollut. 27 (2000) 2–19.
[6] H.J. Zhang, D.Z. Wen, Surf. Coat. Technol. 201 (2007) 5720–5723.
[7] H. Szymanowski, A. Sobczyk, M. Gazicki-Lipman, W. Jakubowski, L. Klimek, Surf. Coat. Technol. 200 (2005) 1036–1040.
[8] H.M. Coleman, C.P. Marquis, J.A. Scott, S.-S. Chin, R. Amal, Chem. Eng. J. 113 (2005) 55–63.
[9] S.H. Si, K.L. Huang, X.G. Wang, M.Z. Huang, H.F. Chen, Thin Solid Films 422 (2002) 205–210.
[10] S. Tanemra, L. Miao, W. Wunderlich, M. Tanemura, Y. Mori, S. Toh, K. Kaneko, Sci. Technol. Adv. Mater. 6 (2005) 11–17.
[11] L. Miao, S. Tanemura, Y. Kondo, M. Iwata, S. Toh, K. Kaneko, Appl. Surf. Sci. 238 (2004) 125–131.
[12] K. Guan, Surf. Coat. Technol. 191 (2005) 155–160.
[13] L. Ge, M. Xu, H. Fang, Thin Solid Films 515 (2007) 3414–3420.
[14] R. Mori, M. Takahashi, T. Yoko, J. Mater. Res. 21 (2006) 270–275.
[15] R. Mori, M. Takahashi, T. Yoko, J. Mater. Res. 20 (2005) 121–127.
[16] J.-X. Liu, D.-Z. Yang, F. Shi, Y.-J. Cai, Thin Solid Films 429 (2003) 225–230.
[17] R. Asahi, T. Morikawa, T. Ohwaki, K. Aoki, Y. Taga, Science 293 (2001) 269–271.
[18] T. Morikawa, R. Asahi, T. Ohwaki, K. Aoki, Y. Taga, Jpn. J. Appl. Phys. 40 (2001) L561–L563.
[19] M.H. Habibi, N. Talebian, J.-H. Choi, Dyes Pigments 73 (2007) 103–110.
[20] U. Backman, A. Auvinen, J.K. Jokiniemi, Surf. Coat. Technol. 192 (2005) 81–87.
[21] H. Lin, C.P. Huang, W. Li, S. Ismat Shah, Y.-H. Tseng, Appl. Catal. B 68 (2006) 1–11.
[22] J. Akedo, J. Am. Ceram. Soc. 89 (2006) 1834–1839.
[23] J. Akedo, M. Lebedev, Jpn. J. Appl. Phys. 38 (1999) 5397–5401.
[24] J. Ryu, J.-J. Choi, B.-D. Hahn, D.-S. Park, W.-H. Yoon, K.-H. Kim, Appl. Phys. Lett. 90 (2007) 152901.
[25] J.-J. Choi, B.-D. Hahn, J. Ryu, W.-H. Yoon, D.-S. Park, J. Appl. Phys. 102 (2007) 044101.
[26] J.-J. Choi, J.-H. Lee, D.-S. Park, B.-D. Hahn, W.-H. Yoon, H.-T. Lin, J. Am. Ceram. Soc. 90 (2007) 1926–1929.
[27] N. Xu, Z. Shi, Y. Fan, J. Dong, J. Shi, M.Z.-C. Hu, Ind. Eng. Chem. Res. 38 (1999) 373–379.
[28] B. Ohtani, Y. Ogawa, S. Nishimoto, J. Phys. Chem. B 101 (1997) 3746–3752.
[29] C.B. Almquist, P. Biswas, J. Catal. 212 (2002) 145–156.
[30] R.I. Bickley, T. Gonzalez-Carreno, J.S. Lees, L. Palmisano, R.J.D. Tilley, J. Solid State Chem. 92 (1991) 178–190.
[31] V.M. Naik, D. Haddad, R. Naik, J. Benci, G.W. Auner, Solid-State Chemistry of Inorganic Materials IV MRS Proceedings, vol. 755, 2002, p. DD11.15.
[32] H. Irie, S. Washiuka, N. Yoshino, K. Hashimoto, Chem. Commun. (2003) 1298–1299.